Ridge network in crumpled paper

Christian André Andresen* and Alex Hansen†
Department of Physics, Norwegian University of Science and Technology, N-7491 Trondheim, Norway

Jean Schmittbuhl‡
Institut de Physique du Globe Strasbourg, 5 rue René Descartes, 67084 Strasbourg, France
(Received 20 February 2007; revised manuscript received 1 June 2007; published 20 August 2007)

The network formed by ridges in a straightened sheet of crumpled paper is studied using a laser profilometer. Square sheets of paper were crumpled into balls, unfolded, and their height profile measured. From these profiles the imposed ridges were extracted as networks. Nodes were defined as intersections between ridges, and links as the various ridges connecting the nodes. Many network and spatial properties have been investigated. The tail of the ridge length distribution was found to follow a power law, whereas the shorter ridges followed a log-normal distribution. The degree distribution was found to have an exponentially decaying tail, and the degree correlation was found to be disassortative. The facets created by the ridges and the Voronoi diagram formed by the nodes have also been investigated.

DOI: 10.1103/PhysRevE.76.026108 PACS number(s): 89.75.Hc, 83.60.−a, 89.75.Fb, 42.62.−b

I. INTRODUCTION

The crumpling of paper is an everyday occurrence, yet it is a surprisingly rich and complex process. Paper is an elastic, flexible, and heterogeneous material, and many authors have tried to describe its crumpling properties analytically [1–3], numerically [4,5], and experimentally [6–11]. The crumpling process of paper is also interesting because it is a special case of the thin plate deformation problem that is central in describing processes that occur, for example, in car crashes and tank failures [12]. Earlier studies have tried to describe the ridge network of crumpled paper [4,6,10] and some results have been found; however, much is still unclear. This work aims at describing the ridge network formed during the common hand-crumpling process of ordinary printing paper. The application of modern network theory [13–15] has been specially emphasized.

This paper is organized as follows. In Sec. II the experimental procedure is described, and in Sec. III the ridge detection method is presented. The results are discussed in Sec. IV; in particular the ridge length and the degree distribution are discussed. Also, the degree-degree correlation, the clustering, and the surface roughness are investigated, in addition to the facet distribution and the angular ridge distribution. Finally the main conclusions are summarized in Sec. V.

II. EXPERIMENTAL PROCEDURE

Ordinary printing paper was used for all the experiments, and some of the properties of the paper are given in Table I. All the samples were cut into square sheets of 21×21 cm^2, and crumpled by hand into small balls. The diameters of the various balls produced are given in Table I. The hand-crumpling procedure has been applied before [6,8,10], and is practical because it is easy to conduct and produces a compact result. Unfortunately, the process in not repeatable and poorly controlled. Several test crumplings were conducted before the measured samples were crumpled in order to reduce the variance between the samples. Earlier studies [8] on acoustic emissions from crumpling of various materials have indicated that the emission spectra show a surprisingly low sensitivity to the crumpling method. This may indicate that the outcome of the crumpling is not highly sensitive to the details of the process. Balankin *et al.* [10] discuss the scaling behavior of the crumpling process for different paper thicknesses. They conclude that the impact of the variation of the applied confinement force F on the ball radius R is small since there is only a weak dependence $R\propto F^{-0.25}$. For these reasons, no special precautions, such as dents or initial folding, were taken to increase repeatability. After crumpling the samples, they were carefully unfolded, taking care not to tear the paper, introduce new ridges, or remove some of the original ridges. When the paper ball was unfolded the paper was stretched to a size of 20×20 cm^2, and fastened to an aluminum plate. This ensured that the vertical heights of the

TABLE I. List of samples investigated. x and y steps are the numbers of measured points in the x and y directions, respectively. Thickness is the thickness of the paper, and ball diameter is the diameter of the ball produced during the crumpling process. All samples were originally 21×21 cm^2 and thereafter unfolding and stretching to 20×20 cm^2 producing a maximum height of 12 mm. An area of 18×18 cm^2 in the center of the samples was measured.

Sample	x step	y step	Thickness (μm)	Weight (g/m^2)	Ball diameter (mm)
1	900	900	51±5	49.0±1.0	26±2
2	1800	1800	51±5	50.0±1.0	27±2
3	1000	1000	95±5	80.0±0.5	35±2
4	900	900	95±5	80.0±0.5	32±2
5	3600	3600	100±2	83.0±0.5	33±2
6	900	900	220±5	175.0±1.0	43±2

*Christian.Andresen@ntnu.no
†Alex.Hansen@ntnu.no
‡Jean.Schmittbuhl@eost.u-strasbg.fr

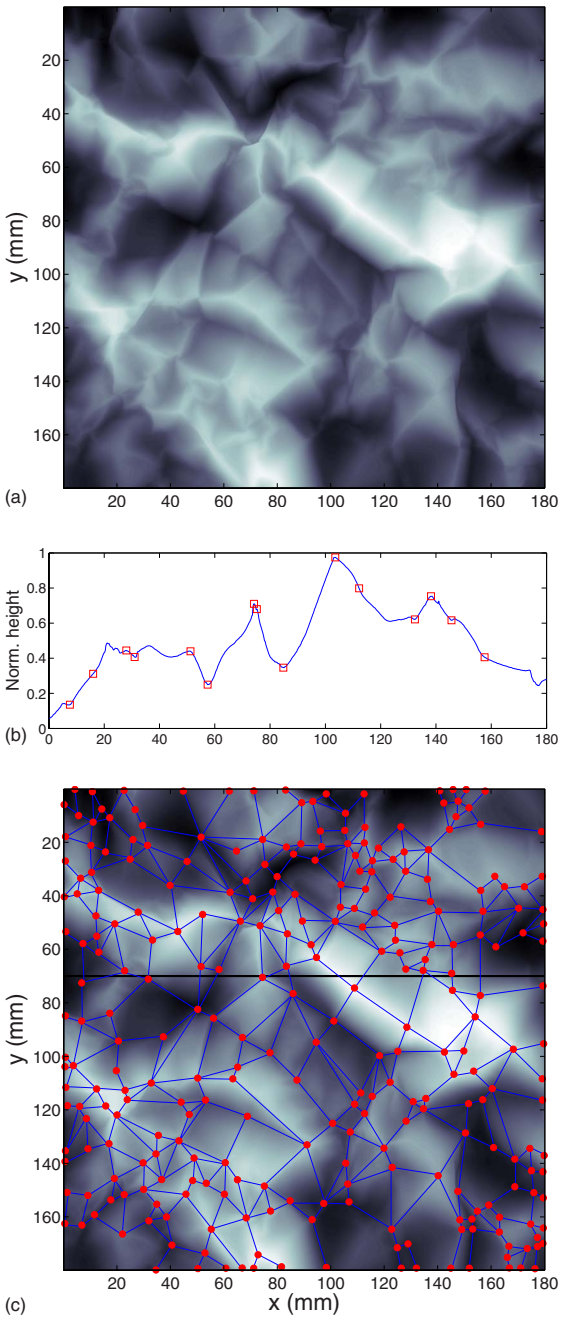

FIG. 1. (Color online) Top: Gray-scale height plot of sample 6 as function of x and y positions. Gray-scale indicates elevation (lighter is higher); ridges are clearly visible. Middle: A single one-dimensional profile from sample 6 (marked as a black line in the bottom plot). The points of the profile that give rise to ridges are marked by squares. Bottom: Network extracted from sample 6 superimposed on the gray-scale plot from the top figure.

samples were no more than 12 mm (the maximum range for the instrument used).

The full (2+1)-dimensional height mapping was measured profile by profile using a laser profilometer over an area of 18×18 cm^2 in the center of the samples. The height of each point was measured using a laser giving a voltage output linearly proportional to the distance between the probe and the paper surface. The voltage output was converted to a floating point length measure using a 16-bit analog-to-digital converter. The laser diameter used was 30 μm; however, accuracy considerably smaller than this could be achieved. Each profile was acquired by sliding the sample under the probe while measuring. Multiple profiles were acquired by stepping the probe normal to the sliding direction. A typical one-dimensional height profile and a complete (2+1)-dimensional map are shown in Fig. 1. The number of points per profile was kept equal to the number of profiles, resulting in a square grid of measurements or "pixels." The number of points used for the various samples is given in Table I. The in-plane accuracy of each point was no larger than 10 μm for any sample, and in the out-of-plane direction it was 0.5 μm for all samples.

III. RIDGE DETECTION

A ridge stands out as a line of high curvature in an otherwise smooth landscape. The curvature of any point in a height profile $\xi(\vec{x})$ can be calculated as the field $\nabla^2\xi(\vec{x})$, where $\vec{x}=(x,y)$ are the planar coordinates. In the present case, it proved necessary to smooth the height profile $\xi(\vec{x})$ with a short-range Gaussian filter before calculating $\nabla^2\xi(\vec{x})$ in order to filter away small-scale features. A range of different filters was tested, and the result did not seem sensitive to the details of the filter. The main effect of the filtering was the removal of single isolated high-curvature pixels, or small groups of such, and a narrowing of the ridge lines. After filtering, the curvature field was calculated and thresholded so that all points over a given value were considered to have a unit value and all other points to have a zero value. Any isolated points above the threshold were filtered away. From the remaining points, lines were detected as ridges. It is throughout this paper assumed that all ridges are straight lines. It proved difficult to automate the ridge extraction process from the thresholded field; finally this step had to be done manually. Some statistics of the produced networks are listed in Table II. Figure 1 shows an example of a full ridge network. In the middle plot of Fig. 1, a single one-dimensional profile is given, and all points along this profile giving rise to ridges are marked. It can be seen from this figure that not all sections of the profile that have high curvature give rise to a ridge, while some smooth sections do give rise to a ridge. This may stem from the directionality of the ridges relative to the profile shown. Ridges crossing the profile at a small angle may seem smooth, but small local dents crossing close to orthogonally may seem large.

Nodes are defined as intersections between ridges, and a ridge therefore extends only from one node to another. All the links are regarded as undirected since a paper ridge does not have any preferred direction. The networks formed are fully connected and have therefore only one component.

IV. NETWORK PROPERTIES

The different paper thicknesses used in the experiments showed a clear trend that thinner paper crumple more than thick paper, and therefore produce more nodes and links (see Tables I and II). Apart from the scale of the network created,

TABLE II. List of extracted networks with their number of nodes, number of links, clustering coefficient C, the clustering coefficient for the corresponding planar Delaunay network, C_D, the clustering coefficient for a nonplanar randomized network with the same degree distribution, C_R, and the maximum node degree for the network. The clustering coefficients for the random networks were calculated using an average over 1000 samples after each sample had 10 000 random rewirings.

Sample	Nodes	Links	C	C_D	C_R	Maximum Degree
1	503	890	0.182	0.4371	0.0045	8
2	1211	2238	0.190	0.4315	0.0020	9
3	190	293	0.138	0.4458	0.0095	6
4	350	580	0.162	0.4394	0.0064	8
5	929	1829	0.231	0.4326	0.0029	10
6	286	501	0.199	0.4384	0.0083	8

no significant differences in the various distributions referred to below were detectable. As a consequence, most distributions are averaged over all samples after each of them have been normalized appropriately. The lack of change in the behavior due to sample thickness may arise from the small amount of data available, and no correspondence between paper thickness and other properties can be excluded. From a scaling point of view, a qualitative change of behavior is not expected since a large and thick sheet of paper is equivalent to a thin and small sheet. Note that the needed confinement also varies with the paper thickness, and all our experiments are conducted at approximately the same confinement. Sultan and Boudaoud [11] discuss two regimes for the crumpling process, depending on the confinement of the sample. The transition confinement is partly dependent on the paper thickness. Our experiments are as mentioned conducted at approximately constant confinement (although it is poorly controlled), and it might therefore be that due to the varying paper thickness our samples lie in different regimes. However, the uniform behavior of the samples indicates that they are all in the same regime. Also the number of self-contacts is very large for all the samples, and this indicates that they are all in the highly confined regime.

It can be seen from Table I that samples 3 and 4 both have the same paper thickness, although they have significantly different numbers of links and nodes. This is most likely due to the difference in confinement. Sample 3 had a larger ball radius than sample 4, and was therefore less confined, and also has fewer nodes and links than sample 4.

A. Ridge length

The length of a ridge between nodes a and b is defined as the spatial length from node a to b, following the assumption that all ridges are straight lines. Previous works have reported log-normal, Γ, and exponential functions [3,6,10] to give good fits for this distribution. However, we find that, whereas the small-scale part of the distribution is well fitted by a log-normal function, the tail of the distribution is not well fitted by any of the above-mentioned functions. The

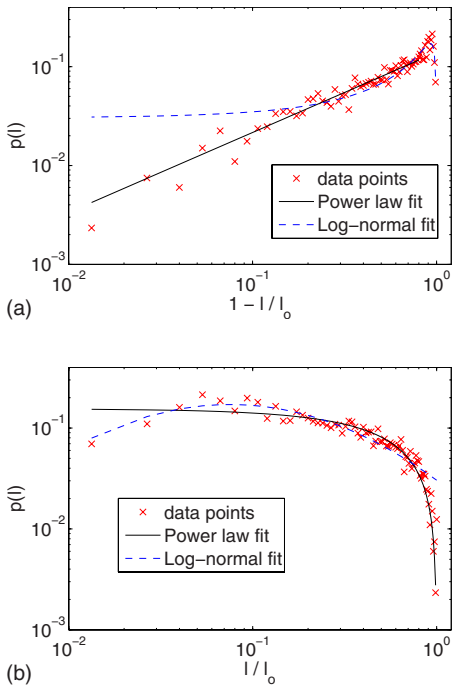

FIG. 2. (Color online) (a) Plot of the average noncumulative ridge length distribution $p(l)$ as a function of $1-l/l_0$, where l is the ridge length and l_0 is the maximum ridge length for any given sample. The data are fitted by a log-normal distribution and a power law $p(l) \propto (1-l/l_0)^{\beta}$ with $\beta=0.81$. (b) Plot of the average noncumulative ridge length distribution $p(l)$ as a function of normalized ridge length l/l_0.

large-scale part of the distribution is better fitted by a power-law function $p(l) \propto (1-l/l_0)^{\beta}$ where l is the ridge length and l_0 is the maximum ridge length for a given sample. Both fits can be seen in Fig. 2. We have found the tail to be best fitted by an exponent $\beta=0.81$. To compare the fits of the different functions they are plotted in Fig. 3 divided by the original distribution in order to emphasize any discrepancies.

The underlying reason for the shift in behavior may stem from the fact that the distribution of short ridges is dominated by remnants of originally long ridges. These ridges have been intersected by "younger" ridges crossing them after their formation. As outlined by Blair and Kudrolli [6], this random sectioning of ridges will give rise to a log-normal length distribution. The larger ridges, on the other hand, have not been so heavily sectioned by younger ridges. They are therefore not expected to follow the log-normal distribution of the shorter ridges. Instead, we detect a power-law dependency of the distribution of the difference between the longest ridge l_0 and the ridge length. It is reasonable to assume that larger samples will produce larger maximum ridges, and therefore l_0 is a sample-size-dependent quantity. Why this difference should exhibit a scale-free behavior is not clear.

B. Degree distribution

The degree of a node is defined as the number of ridges meeting at that node. The distribution has been found to have

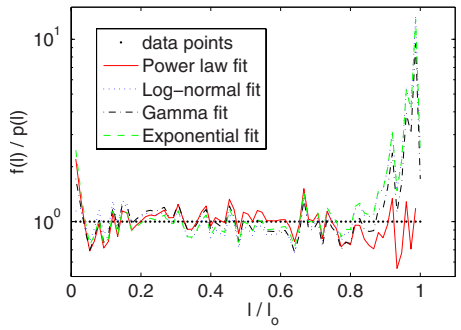

FIG. 3. (Color online) For comparison, the results shown in Fig. 2 from fitting the ridge length distribution $p(l)$ with Γ, log-normal, and exponential functions divided by the data themselves are shown, together with the same plot for the power-law fit as a function of normalized ridge length l/l_0.

a maximum probability at a median degree and produce a Gaussian-like form that is plotted in Fig. 4. The tail of the distribution is well fitted by a log-normal function of the same form as in Eq. (4). This is in strong contrast to many naturally occurring networks, which show a power-law tail, giving a larger portion of high-degree nodes than can be seen in the acquired samples.

C. Degree-degree correlation

The correlation between the degree of connected nodes has been studied using the procedure developed by Maslov and Sneppen [15]. They have defined a correlation measure

$$C(k_1,k_2) = \frac{P(k_1,k_2)}{P_R(k_1,k_2)}, \tag{1}$$

where $P(k_1,k_2)$ is the probability that a node of degree k_1 is linked to a node of degree k_2. $P_R(k_1,k_2)$ is the same average probability for a set of randomized networks. The randomized networks are assumed to have the same numbers of nodes and links, and the same degree distribution as the original network. A value $C(k_1,k_2)>1$ indicates that there is an over-representation of links between nodes with degree k_1 and k_2, whereas $C(k_1,k_2)<1$ indicates an under-representation. In order to look at the statistical signification of the correlation, Maslov and Sneppen introduced another correlation measure,

$$Z(k_1,k_2) = \frac{P(k_1,k_2) - P_R(k_1,k_2)}{\sigma_R(k_1,k_2)}, \tag{2}$$

where $\sigma_R(k_1,k_2)$ is the standard deviation of the samples used to generate $P_R(k_1,k_2)$. For $P(k_1,k_2)$ only the sample data are available. If a given coupling $P(k_1,k_2)$ is over-represented [that is, $P(k_1,k_2)>P_R(k_1,k_2)$] then $Z(k_1,k_2)>0$ and if it is under-represented $Z(k_1,k_2)<0$. If the standard deviation is small, the corresponding correlation coefficients are large, thus emphasizing statistically significant results. In all results presented here, 1000 randomized versions of the various samples were used to produce $P_R(k_1,k_2)$ and $\sigma_R(k_1,k_2)$. Each randomization used 10 000 rewirings of the original network.

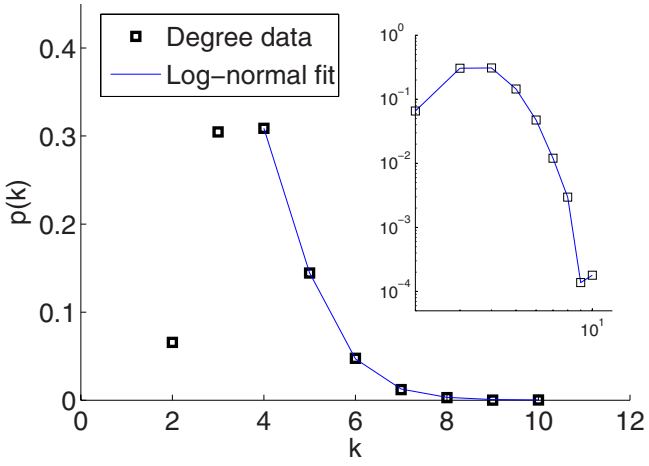

FIG. 4. (Color online) Plot of the degree distribution $p(k)$ as a function of node degree k with a fitted log-normal tail. The inset shows the same data plotted on log-log scale. This shows that the distribution does not have a power-law-distributed tail.

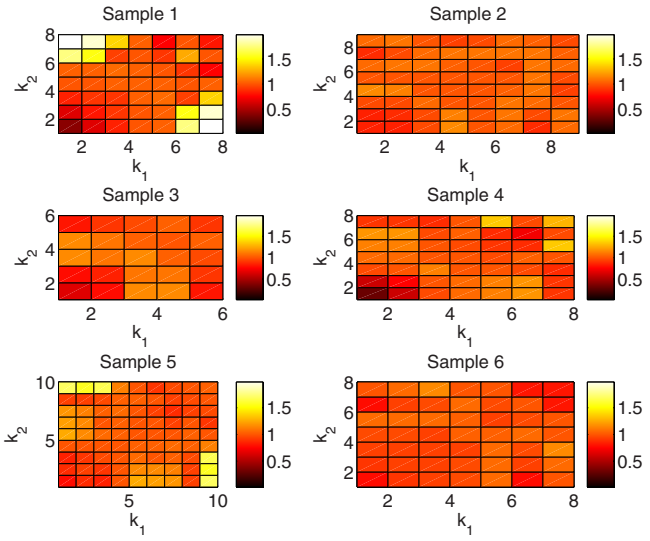

FIG. 5. (Color online) Correlation matrix $C(k_1,k_2) = P(k_1,k_2)/P_R(k_1,k_2)$ for each sample. The plots indicate that the networks are disassortative.

Figure 5 shows the $C(k_1,k_2)$ matrix for all the samples. There is a tendency of small-degree nodes not to link to other small-degree nodes, but rather link to large-degree nodes. Links between large-degree nodes are also under-represented. This type of network is known as a disassortative network. Figure 6 shows the $Z(k_1,k_2)$ matrices for the same samples, and the same trends as in Fig. 5 can be observed. There is a clear trend in nearly all examined networks [16] that technical and biological networks such as the Internet and various protein interaction networks are disassortative, and that social networks such as acquaintance networks are assortative. The underlying reason for this is still not fully understood.

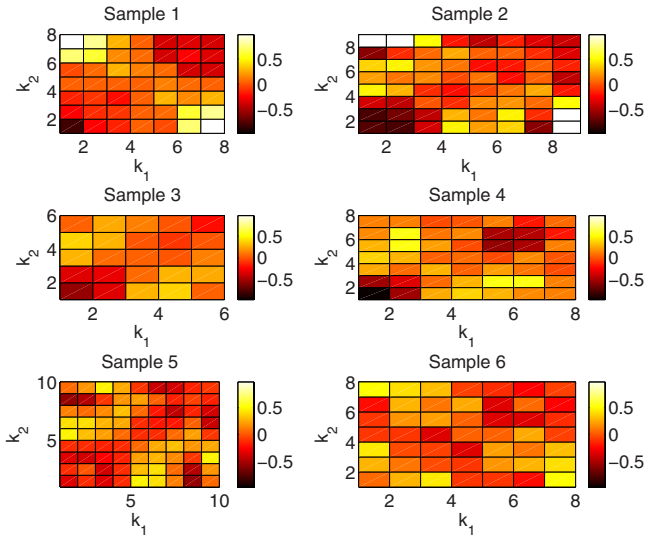

FIG. 6. (Color online) Z matrix $Z(k_1,k_2)=[P(k_1,k_2)-P_R(k_1,k_2)]/\sigma_R(k_1,k_2)$ for each sample. As in the $C(k_1,k_2)$ case of Fig. 5, the plot indicates a disassortative trend.

D. Clustering

The cluster coefficients C for all the samples are given in Table II, and they are all in the range 0.13–0.23. The definition used here is the standard

$$C = \frac{1}{N}\sum_{i=1}^{i=N} C_i, \tag{3a}$$

$$C_i = \frac{2E_{\mathrm{NN}}}{k_i(k_i-1)}, \tag{3b}$$

where N is the number of nodes in the network, E_{NN} is the number of links between nearest neighbors of node i, and k_i is the degree of node i [14]. A network embedded in two-dimensional Euclidean space with no crossing links is called a *planar network*, and has been described by West [17]. Generating a planar randomized network for comparing the cluster coefficients is very hard since no links can cross and the rewiring therefore must be local. However, the clustering can be compared with the Delaunay network [18] for the same spatial layout of nodes. For a given spatial node configuration and degree distribution, the Delaunay network gives the maximum possible clustering coefficient. The clustering coefficient for a Delaunay network made from nodes randomly distributed in the plane and with a number of nodes comparable to our samples is 0.44. Delaunay networks are closely linked to Voronoi diagrams, and both are described below. The cluster coefficient for a nonplanar random network, where the links can cross, having the same number of nodes and links and the same degree distribution is in the order of 0.001. The ridge networks have a much higher clustering than the nonplanar networks. This is expected because any node in a planar network has a low chance of being linked to a faraway node. This will generally increase the local clustering [17]. On the other hand the clustering is significantly lower than in the Delaunay case. This indicates that the ridge network does not form highly interconnected cliques.

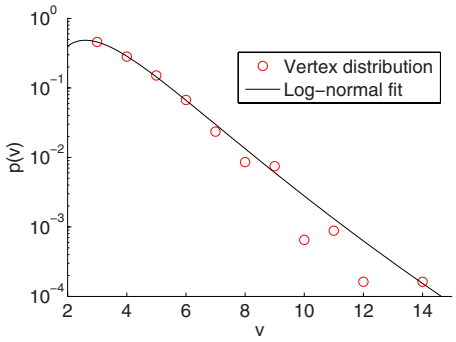

FIG. 7. (Color online) Average vertex distribution $p(v)$ as a function of the number of vertices v for the facets formed by the ridges. The data are fitted to a log-normal function with $\sigma=0.42$ and $\mu=1.13$.

V. GEOMETRICAL PROPERTIES

Various geometrical properties of crumpled thin sheets have been investigated in the past [6,19,20]. Here we discuss the size distribution of facets formed by the ridges and of the Voronoi sections formed by the location of the nodes. The angular distribution of the ridges and the three-cone structures is also investigated.

A. Facets

The nodes and links of the network form facets (also called domains) of various sizes and shapes. A facet is defined as an area of the crumpled paper confined by a closed loop of ridges that is simply connected, meaning that it contains no internal facets. The nodes bordering the facets are the corners or vertices of the facet. The distribution of facet areas and number of vertices for each sample have been calculated. The vertex distribution for all the samples was averaged, giving each sample equal weight. The number of facets with three, four, five, and six vertices was 46%, 28%, 15%, and 8%, respectively, and the number of facets with more than six vertices was 4%. The maximum number of vertices was 14. In Fig. 7 the distribution of the facet vertex number can be seen; the data are fitted with a log-normal function

$$p(a) = \frac{1}{\sqrt{2\pi}a\sigma} e^{-[\ln(a)-\mu]^2/(2\sigma)^2}, \tag{4}$$

where a is the vertex number, μ is the logarithm of the average number of vertices per facet, and σ is the standard deviation. The best fit was achieved with $\sigma=0.42$ and $\mu=1.13$.

The areas of the facets have also been investigated. The binned distribution of areas was normalized by the maximum area for each sample, and the average over all samples calculated. The resulting distribution can be seen in Fig. 8 together with a log-normal fit. The best fit parameters were $\sigma=1.17$ and $\mu=2.16$ in arbitrary units.

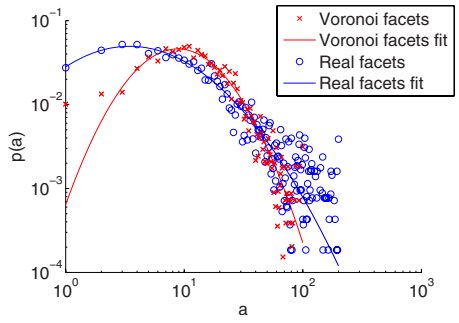

FIG. 8. (Color online) Average area distribution $p(a)$ as a function of the facet area a for the facets formed by the ridges and the Voronoi regions. Both sets of data are fitted by a log-normal function with $\sigma=1.17$ and $\mu=2.61$ for the facets and $\sigma=0.74$ and $\mu=2.73$ for the Voronoi regions, both in the same arbitrary units of area.

B. Voronoi networks

Given a set of nodes in space (or the plane) the Voronoi diagram [18] is a sectioning into areas around each node where each section contains all the points that are closest to the node in its interior. This partitions space (the plane) into sections filling the whole space (plane). The Delaunay network is a network where each node is linked to all the other nodes that it shares a Voronoi section border with. A visualization of this is given in Fig. 9, where the Voronoi diagrams for four of the samples are plotted. The gray scale of a given Voronoi section reflects the size of the section. Smaller sections have a lighter shade and larger sections have a darker shade. It can be seen that the sections are grouped according to size, making regions of the whole diagram that contains mainly large or small sections. The distributions of the areas of the various Voronoi sections have been calculated and fitted with a log-normal function. As in the facet case, each sample has been normalized by its maximum area. The distribution follows the same general shape as the facet distribution, and they can both be seen in Fig. 8.

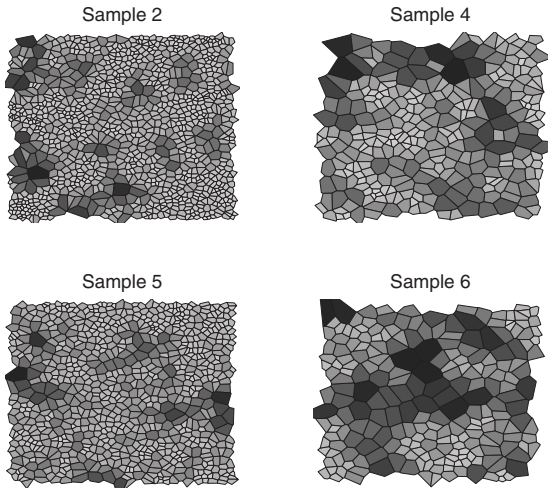

FIG. 9. Voronoi diagrams for four samples. The gray shading of the various sections represents the area of the sections. Lighter areas are smaller. There is a clear trend for sections of small (large) size to group with other small- (large-)sized sections.

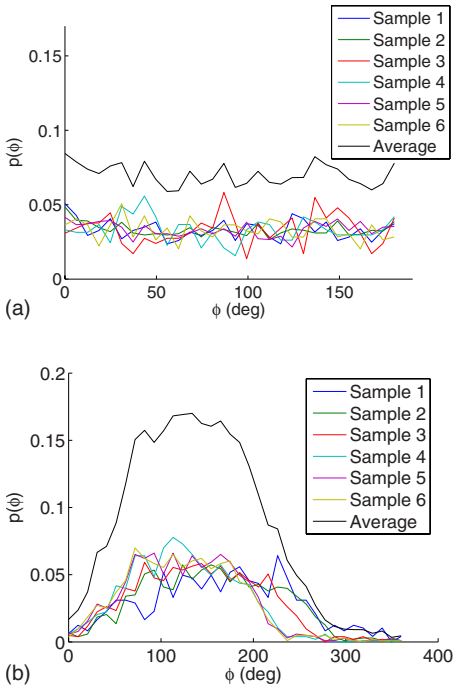

FIG. 10. (Color online) (a) Distribution of ridge angles, $p(\phi)$, as a function of angle ϕ for all the samples and the average (elevated for clarity). No trend is visible in the plot. (b) Distribution of separation angles, $p(\phi)$, as a function of opening angle ϕ in three ridge nodes. The average is elevated for clarity.

C. Angular distribution

The angular distribution of the ridges relative to the border of the sample has been studied in order to detect any preferred ridge direction or ordering among the ridges with regard to direction. No such preferred direction or ordering was found, and the distribution of ridge angles was reasonably uniform, both for each sample and for the average. A plot of the binned ridge angle distribution can be seen in Fig. 10.

The distribution of angles between ridges in a three-ridge cone (a node where three ridges meet, and hence form a conelike structure) has earlier been investigated both analytically and experimentally [6,19,20]. It has been reported that there are indications of preferred opening angles for such cones in the regions about 20°, 60°, and 110°, although all acquired distributions have been broad. All $k=3$ nodes have been investigated and the ridge separation angles show a broad distribution with a maximum in the range between 100° and 150°. There are no significant peaks in the distribution and this indicates a random ordering. However, 32% of all the angles lies in the interval between 90° and 150°. This suggests that the ridges tend to span out, trying to separate themselves from each other. Recall that 120° is the angle at which they are evenly separated. A plot of the distribution for all the samples and their average can be seen in Fig. 10.

VI. ROUGHNESS

The roughness of crumpled paper surfaces has been investigated before [4,6,10]. These investigations have reported self-affine behavior; this means that the surface is statistically characterized by

$$h(x) = \lambda^{-H} h(\lambda x), \tag{5}$$

where $h(x)$ is the height of the profile at position x, λ is a rescaling factor, and H is the Hurst exponent. We have investigated the one-dimensional profiles produced by the profilometer using the average wavelet coefficient (AWC) method [21], the power spectrum density (PSD) method [22], and the bridge method [23]. The results from all the methods indicate that the crumpled paper forms a self-affine surface. Earlier works have reported a small-scale region with a Hurst exponent $H_S \sim 1.0$ and a large-scale region with $H_L \sim 0.7$ [6,10] and $H_L \sim 0.8$ [4]. Our results follow the same trend in that there is a crossover scale between two scaling regimes. However, we found the small-scale exponent to be $H_S = 1.25 \pm 0.05$, indicating that the surface is asymptotically nonflat at these scales. Unfortunately, the data did not give a robust value for H_L because the sample size was too small compared to the crossover scale. The data did, however, indicate that $H_L < 1.0$ and in the range reported above. In Fig. 11, results from the PSD and AWC methods can be seen.

VII. CONCLUSION

The main points reported above are that the tail of the ridge length distribution is found to be well reproduced by a power-law distribution, and that the short ridges follow a log-normal distribution as reported earlier. The degree distribution has been shown not to have a power-law tail, but rather an exponential decay, and the networks have been found to be disassortative. The facet area distribution, the corresponding Voronoi diagram area distribution, and the Delaunay vertex distribution have all been found to fit log-normal distributions.

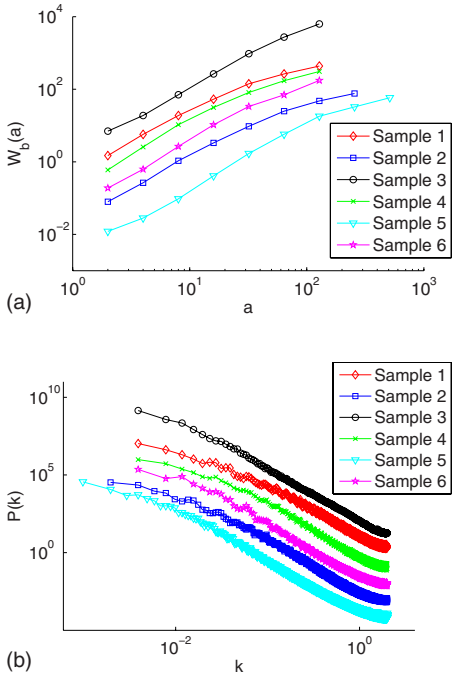

FIG. 11. (Color online) (a) Results from the AWC analysis showing the average wavelet coefficients $W_b(a)$ as a function of scale a; the scale represents measured points. (b) Results from the PSD analysis showing the power spectrum density $P(k)$ as a function of spatial frequency k. In both (a) and (b) the data sets are vertically shifted for clarity.

ACKNOWLEDGMENTS

This work have been supported by VISTA, a research cooperation between the Norwegian Academy of Science and Letters and Statoil. We would also like to thank J. Ø. Bakke and R. Toussaint for fruitful discussions, and the referees for valuable input.

[1] M. Ben Amar and Y. Pomeau, Proc. R. Soc. London, Ser. A **453**, 729 (1997).
[2] A. E. Lobkovsky and T. A. Witten, Phys. Rev. E **55**, 1577 (1997).
[3] A. J. WoodPhysica A **313**, 83 (2002).
[4] F. Plouraboué and S. Roux, Physica A **227**, 173 (1996).
[5] G. A. Vliegenthart and G. Gompper, Nat. Mater. **5**, 216 (2006).
[6] D. L. Blair and A. Kudrolli, Phys. Rev. Lett. **94**, 166107 (2005).
[7] L. Boué, M. Adda-Bedia, A. Boudaoud, D. Cassani, Y. Couder, A. Eddi, and M. Trejo, Phys. Rev. Lett. **97**, 166104 (2006).
[8] P. A. Houle and J. P. Sethna, Phys. Rev. E **54**, 278 (1996).
[9] J. P. Sethna, K. A. Dahmen, and C. R. Myers, Nature (London) **410**, 242 (2001).
[10] A. S. Balankin, O. S. Huerta, R. Cortes Montes de Oca, D. S. Ochoa, J. Martinez Trinidad, and M. A. Mendoza, Phys. Rev. E **74**, 061602 (2006).
[11] E. Sultan and A. Boudaoud, Phys. Rev. Lett. **96**, 136103 (2006).
[12] A. E. Lobkovsky, S. Gentges, H. Li, D. Morse, and T. A. Witten, Science **270**, 1482 (1995).
[13] S. Boccaletti, V. Latora, Y. Moreno, M. Chavez, and D.-U. Hwang, Phys. Rep. **424**, 175 (2006).
[14] M. E. J. Newman, SIAM Rev. **45**, 167 (2003).
[15] S. Maslov and K. Sneppen, Science **296**, 910 (2002).
[16] Eur. Phys. J. B **38**, 143 (2004), special issue on ten leading questions for network research.
[17] D. B. West, *Introduction to Graph Theory* (Prentice-Hall, Englewood Cliffs, NJ, 1995).
[18] F. Aurenhammer, ACM Comput. Surv. **23**, 345 (1991).
[19] E. Cerda and L. Mahadevan, Phys. Rev. Lett. **80**, 2358 (1998).

[20] S. Chaïeb, F. Melo, and J. C. Geminard, Phys. Rev. Lett. **80**, 2354 (1998).
[21] I. Simonsen, A. Hansen, and O. M. Nes, Phys. Rev. E **58**, 2779 (1998).
[22] A. R. Mehrabi, H. Rassamdana, and M. Sahimi, Phys. Rev. E **56**, 712 (1997).
[23] T. Engøy, K. J. Måløy, A. Hansen, and S. Roux, Phys. Rev. Lett. **73**, 834 (1994).